

# Large Electron Model: A Universal Ground State Predictor

Timothy Zaklama,<sup>1,\*</sup> Max Geier,<sup>1</sup> and Liang Fu<sup>1,†</sup>

<sup>1</sup>*Department of Physics, Massachusetts Institute of Technology, Cambridge, Massachusetts 02139, USA*

We introduce *Large Electron Model*, a single neural network model that produces variational wavefunctions of interacting electrons over the entire Hamiltonian parameter manifold. Our model employs the Fermi Sets architecture [1], a universal representation of many-body fermionic wavefunctions, which is further conditioned on Hamiltonian parameter and particle number. On interacting electrons in a two-dimensional harmonic potential, a single trained model accurately predicts the ground state wavefunction while generalizing across unseen coupling strengths and particle-number sectors, producing both accurate real-space charge densities and ground state energies, even up to 50 particles. Our results establish a foundation model method for material discovery that is grounded in the variational principle, while accurately treating strong electron correlation beyond the capacity of density functional theory.

## INTRODUCTION

A central goal of materials science is to predict new properties of matter before they are measured. If this goal were achieved at scale, it would change how we discover materials, design molecules, and engineer quantum devices. While trial and error dominates the domain, accurate prediction of candidate materials with targeted functionality could transform materials research. The rise of artificial intelligence (AI) raises the question: can AI predict new, experimentally verifiable material properties? So far, studies in materials through AI have largely relied on existing datasets of experimentally measured material properties. But the properties we ultimately care about—equation of state, transport, magnetism, superconductivity, chemical reactivity—are all determined by the dynamics of interacting electrons as governed by the physical laws of quantum mechanics.

Reliable prediction beyond what has already been measured therefore must come from solving many interacting electrons at scale. This is where progress has been slow for decades: while first-principles electronic structure is the most promising route to reliable prediction, accurate methods remain expensive and system specific. Density functional theory (DFT) has been the workhorse of electronic structure calculations because it is versatile and scalable, enabling routine calculations on systems with a large number of electrons. However, despite its widespread success, DFT is not variational, does not produce many-body ground state wavefunctions, and completely fails in strongly correlated materials such as fractional Chern insulators or strong-coupling superconductors.

Recently, a new approach to solve the many-electron problem using fermionic neural networks (NNs) [2–5] has shown great promise. In particular, self-attention neural networks [6, 7] are shown to accurately represent a wide variety of interacting electron states, including strongly correlated, highly entangled, and topologically ordered quantum matter that cannot be treated by DFT or any

mean-field method [8–12]. More recently, a *provably* universal Fermi network has been found, which is capable of approximating any continuous Fermi wavefunctions to arbitrary accuracy using only a small number of Slater determinants [1].

By optimizing the network parameters through Monte Carlo energy minimization, fermionic NNs are able to solve the many-electron Schrodinger equation variationally, and find an accurate ground state energy and full quantum many-body wavefunction, from which *all* static and thermodynamic properties can be determined. Despite achieving high accuracy on many atomic, molecular and solid-state systems, the prevalent workflow of neural-network variational Monte Carlo still optimizes a new network for each Hamiltonian and each parameter choice from scratch, without the ability to reuse computation across different systems or sizes.

The missing piece is a foundation model approach that solves for the many-electron quantum wavefunction across a manifold of physical settings with one shared set of parameters [13–23]. Broadly speaking, foundation models are trained on diverse and vast data sets to learn to predict beyond the available data. Applied to the materials context, foundation models replace single-instance solvers with parameter-sharing networks that learn transferable structure and enable rapid prediction after training. In our many-electron setting, supervised training is not viable, as the important problems do not come with ground-truth wavefunctions or energies at large system size. For solving the many-electron problem at scale, a viable foundation model must learn unsupervised from the governing physical principle itself.

In this work, we introduce *Large Electron Model*, a foundation model for quantum wavefunctions of many-electron systems in the continuum. We train a single parameter-sharing network that conditions on Hamiltonian parameters, such as interaction strength, and particle number, and directly predicts the ground-state wavefunction for Hamiltonians it never saw. The model is fully unsupervised: it requires no reference solutions, no labeled training data, and no precomputed datasets; it is

trained end-to-end by variational energy minimization. The model is thus an universal ground state predictor that is variational by construction, rivaling the universality of DFT yet surpassing its reach in regimes of strong correlations, and guaranteeing a more interpretable and holistic solution.

Our foundation model is built from a *universal* Fermi wavefunction ansatz, which factorizes the wavefunction into an antisymmetric single-particle component and a symmetric correlation component [1, 24]. The antisymmetric head allows for most general fermionic sign structures through a compact Slater determinant basis, while the symmetric head learns electron correlations through an attention-based network designed to model systems with global dependencies. This architecture, which is both physically motivated and provably universal, yields a lightweight, efficient implementation that is well suited to capturing many-electron ground states from weak to strong interaction regimes.

We demonstrate the power of our foundation model on the quantum dot problem: interacting electrons in a two-dimensional harmonic trap, with variable interaction strengths  $\lambda$ , and particle numbers  $N$ . After training via unsupervised energy minimization across interaction regimes and Hilbert-space sectors in a single run, we showcase the model’s ability to accurately predict the entire family of ground state wavefunctions, whose energy expectation values beats benchmarks set by standard methods. Further, we show the model’s remarkable generalization to predict the entire ground state wavefunction across interaction strength, and, critically, particle-number sectors through real space charge density plots. We also highlight the model’s scalability, generalizing across the full interaction manifold for as large as  $N = 50$  particles. Our results establish a promising path beyond DFT for material discovery based on a universal and variational wavefunction model that can operate at large system sizes, while achieving unprecedented accuracy in strongly correlated regimes where DFT breaks down.

## THEORETICAL FRAMEWORK

We consider a *family* of continuum, many-electron Hamiltonians indexed by parameters  $\Lambda \in \mathcal{P}$  (e.g., interaction strength and particle number). For each  $\Lambda$ , the ground state is a fermionic wavefunction in first quantization,  $\Psi_\Lambda(\mathbf{R}, \mathbf{s})$ , defined on configurations  $\mathbf{R} = (\mathbf{r}_1, \dots, \mathbf{r}_N) \in (\mathbb{R}^d)^N$  with spin labels  $\mathbf{s} = (s_1, \dots, s_N)$ . Fermionic statistics impose antisymmetry under relabeling indistinguishable electrons:

$$\Psi_\Lambda(\pi \cdot \mathbf{R}, \pi \cdot \mathbf{s}) = (-1)^\pi \Psi_\Lambda(\mathbf{R}, \mathbf{s}), \quad \forall \pi \in S_N. \quad (1)$$

where  $S_N$  denotes the permutation group.

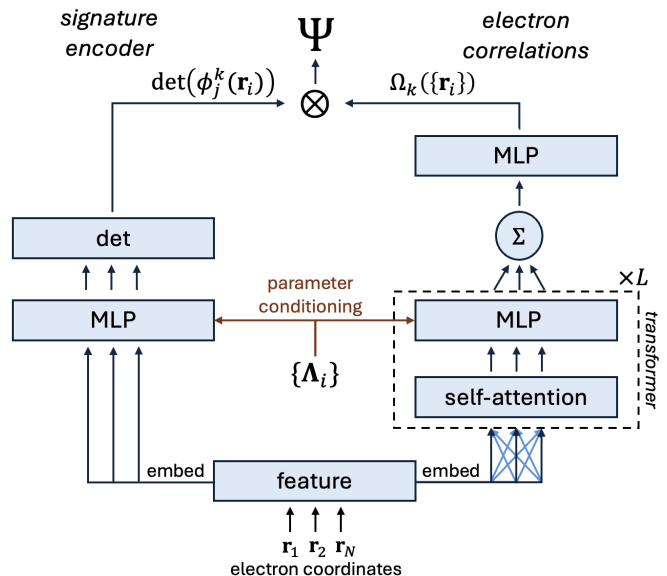


FIG. 1. **Foundation model architecture.** A Multilayer Perceptron (MLP) with determinant head (left) constructs a set of  $K$  signature encoders formulated as Slater determinants with orbitals represented by the MLP. Electron correlations are captured by a permutation-symmetric function represented by a transformer with symmetric head (right). Conditioning both parts with the parameters  $\Lambda_i$  yields the continuous parameterization of the many-body wavefunction  $\Psi_\Lambda(\{\mathbf{r}_i\})$ .

Our goal is to learn a *single* neural wavefunction  $\Psi_\theta$  that represents the entire manifold  $\{\Psi_\Lambda : \Lambda \in \mathcal{P}\}$  of variational ground states by conditioning on  $\Lambda$ :

$$\Psi_\theta : (\mathbf{R}, \mathbf{s}, \Lambda) \mapsto \Psi_\theta(\mathbf{R}, \mathbf{s}; \Lambda) \in \mathbb{C}, \quad (2)$$

with shared parameters  $\theta$  across all  $\Lambda$ . This “parameter-sharing” approach is the defining feature of the foundation model: by training on an ensemble of Hamiltonians, the model learns a structured map  $\Lambda \mapsto \Psi_\theta(\mathbf{R}, \mathbf{s}; \Lambda)$  that can interpolate and generalize beyond the discrete training set. In our problem, the model must learn to interpolate in infinite-dimensional space of  $N$ -particle wavefunctions in continuous space, a daunting task!

We train  $\Psi_\theta$  via the variational principle. For each  $\Lambda$ , define the normalized energy functional

$$E_\theta(\Lambda) = \frac{\langle \Psi_\theta(\mathbf{R}, \mathbf{s}; \Lambda) | \hat{H}(\Lambda) | \Psi_\theta(\mathbf{R}, \mathbf{s}; \Lambda) \rangle}{\langle \Psi_\theta(\mathbf{R}, \mathbf{s}; \Lambda) | \Psi_\theta(\mathbf{R}, \mathbf{s}; \Lambda) \rangle}. \quad (3)$$

In variational Monte Carlo (VMC), this can be written as an expectation over the Born density  $\propto |\Psi_\theta(\mathbf{R}, \mathbf{s}; \Lambda)|^2$  using the local energy  $E_L(\mathbf{R}, \mathbf{s}; \Lambda) = \hat{H}(\Lambda)\Psi_\theta/\Psi_\theta$ . Given a finite training ensemble  $\{\Lambda_g\}_{g=1}^G \subset \mathcal{P}$ , we minimize the

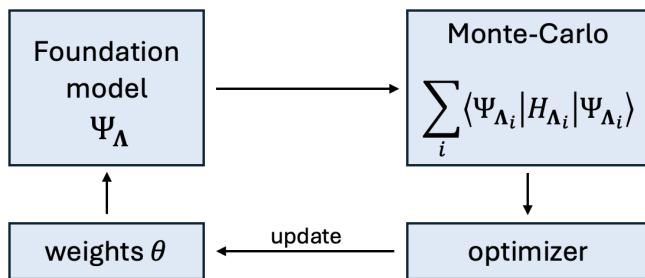


FIG. 2. **Workflow.** The network represents the many-body wavefunction with continuous parameter dependence  $\Psi_{\Lambda}(\{\mathbf{r}_i\})$ . The loss is computed as the total energy  $\sum_i \langle \Psi_{\Lambda_i} | H_{\Lambda_i} | \Psi_{\Lambda_i} \rangle$  accumulated over a fixed set of system parameters  $\{\Lambda_i\}$ , where the individual energy expectation values are computed using Monte-Carlo sampling. From the gradients of the total energy, an optimizer routine determines updates of network weights  $\theta$ .

multi-task objective

$$\mathcal{L}(\theta) = \frac{1}{G} \sum_{g=1}^G E_{\theta}(\Lambda_g) \quad (4)$$

$$= \frac{1}{G} \sum_{g=1}^G \mathbb{E}_{(\mathbf{R}, \mathbf{s}) \sim |\Psi_{\theta}(\mathbf{R}, \mathbf{s}; \Lambda_g)|^2} [E_L(\mathbf{R}, \mathbf{s}; \Lambda_g)]. \quad (5)$$

## APPROACH

We now introduce a universally representative foundation model for interacting fermions in the continuum. The central novelty is a single conditional neural wavefunction that maps Hamiltonian parameters to ground-state wavefunctions for real-space continuum systems, trained once and reused across a manifold of physical settings. To our knowledge, this is the first foundation-model formulation that targets real physical systems in the continuum via an explicitly fermionic, universally representative ansatz.

Let  $N$  electrons in  $d$  dimensions have configuration  $\mathbf{R} = (\mathbf{r}_1, \dots, \mathbf{r}_N)$  with spins  $\mathbf{s} = (s_1, \dots, s_N)$ . Fermi Sets [1] expresses any continuous fermionic wavefunction as a sum of symmetric functions multiplying antisymmetric cores,

$$\Psi_{\theta}(\mathbf{R}, \mathbf{s}; \Lambda) = \sum_{k=1}^K \Omega_{\theta,k}(\mathbf{R}, \mathbf{s}; \Lambda) \eta_{\theta,k}(\mathbf{R}, \mathbf{s}, \Lambda), \quad (6)$$

where each  $\Omega_{\theta,k} \in \mathbb{C}$  is invariant under any permutation of the electron labels, while each  $\eta_{\theta,k}$  is antisymmetric. This factorization guarantees fermionic antisymmetry, while allowing the symmetric prefactors to adapt configuration-by-configuration. Here, we generalize the Fermi Sets to include parameter dependence for the purpose of building a foundation model.

We begin by describing the construction of the symmetric component,  $\Omega_{\theta,k}$ . We define geometric features relative to fixed reference centers  $\{\mathbf{R}_A\}_{A=1}^{N_c}$  (e.g., the center of harmonic trap or the position of a nuclei), to build particle features,

$$\mathbf{a}_{iA} = \mathbf{r}_i - \mathbf{R}_A, \quad r_{iA} = \|\mathbf{a}_{iA}\|, \quad (7)$$

These coordinate features are concatenated with the electron spin to describe spinful wavefunctions [25, 26]. These features are then embedded into a latent space where they are processed by a transformer [7, 27]. At this stage parameter conditioning is introduced to the parameter space  $\Lambda$  [23]. This operation  $h_{\theta}$  on the particle features and parameter space yields the tokens

$$\mathbf{t}_i = h_{\theta}(\{r_{iA}, \mathbf{a}_{iA}\}_{A=1}^{N_c}, s_i; \Lambda) \in \mathbb{R}^f. \quad (8)$$

This output of the transformer is then pooled over the particle index to produce a permutation *invariant* output,

$$\xi_{\theta}(\mathbf{R}, \mathbf{s}; \Lambda) = \sum_{i=1}^N \sigma(\mathbf{t}_i), \quad (9)$$

where  $\sigma$  is a nonlinearity, ensuring  $\xi_{\theta}$  is invariant under electron permutation. For added expressivity, permutation-equivariant weights can be added as coefficients to each term in the sum. The symmetric coefficients are then produced by a small Multilayer Perceptron (MLP)  $\rho_{\theta} : \mathbb{R}^f \rightarrow \mathbb{C}$ :

$$\Omega_{\theta,k}(\mathbf{R}, \mathbf{s}; \Lambda) = \rho_{\theta}(\xi_{\theta}(\mathbf{R}, \mathbf{s}; \Lambda)). \quad (10)$$

For the antisymmetric factor, we choose  $\eta_{\theta,k}$  to be Slater determinants constructed from learned single-particle orbitals [7]:

$$\eta_{\theta,k}(\mathbf{R}, \mathbf{s}; \Lambda) = \det \mathbf{M}_{\theta}^{(k)}(\mathbf{R}, \mathbf{s}; \Lambda),$$

$$[\mathbf{M}_{\theta}^{(k)}(\mathbf{R}, \mathbf{s}; \Lambda)]_{ij} = \phi_{\theta,j}^{(k)}(\mathbf{r}_i, s_i; \Lambda),$$

Antisymmetry is carried entirely by the Slater determinant.

Combining Eqs. (6)–(10) yields the implemented conditional ansatz

$$\Psi_{\theta}(\mathbf{R}, \mathbf{s}; \Lambda) = \sum_{k=1}^K \rho_{\theta}(\xi_{\theta}(\mathbf{R}, \mathbf{s}; \Lambda)) \det \mathbf{M}_{\theta}^{(k)}(\mathbf{R}, \mathbf{s}; \Lambda), \quad (11)$$

which is shown schematically in Fig. 1.

## PHYSICAL SYSTEM

To demonstrate the foundation model framework and its performance in the real world, we study the quantum

dot problem:  $N$  interacting electrons in  $d = 2$  confined by an isotropic harmonic potential, with Coulomb repulsion. Working in atomic units, we consider the standard many-electron Hamiltonian

$$\hat{H}(\mathbf{\Lambda}) = -\frac{1}{2} \sum_{i=1}^N \nabla_i^2 + V_{\mathbf{\Lambda}}(\mathbf{R}), \quad (12)$$

with parametrized potential energy

$$V_{\mathbf{\Lambda}}(\mathbf{R}) = \frac{1}{2} \omega \sum_{i=1}^N \|\mathbf{r}_i\|^2 + \lambda \sum_{i < j} \frac{1}{\|\mathbf{r}_i - \mathbf{r}_j\|}, \quad (13)$$

and parameter vector  $\mathbf{\Lambda} = (N, \omega, \lambda)$ . Here  $\omega$  sets the curvature of the parabolic confinement potential, and  $\lambda$  controls the interaction strength. In all calculations in this work, we set  $\omega = 1$ , which is equivalent to rescaling lengths by  $\mathbf{x}_i = \omega^{1/4} \mathbf{r}_i$  and energies by

$$\hat{H}(N, \omega, \lambda) = \sqrt{\omega} \hat{H}\left(N, 1, \frac{\lambda}{\omega^{1/4}}\right). \quad (14)$$

Thus, results at  $\omega \neq 1$  are obtained from the  $\omega = 1$  solutions through the single dimensionless coupling  $\tilde{\lambda} = \lambda/\omega^{1/4}$  and the overall energy scale  $\sqrt{\omega}$ .

Given  $\Psi_{\theta}(\mathbf{R}, \mathbf{s}; \mathbf{\Lambda})$ , the VMC local energy entering Eq. (5) is

$$E_L(\mathbf{R}, \mathbf{s}; \mathbf{\Lambda}) = \frac{\hat{H}(\mathbf{\Lambda}) \Psi_{\theta}(\mathbf{R}, \mathbf{s}; \mathbf{\Lambda})}{\Psi_{\theta}(\mathbf{R}, \mathbf{s}; \mathbf{\Lambda})}. \quad (15)$$

We train on an ensemble of parameter points  $\{\mathbf{\Lambda}_g\}_{g=1}^G$  spanning a target manifold, thereby optimizing a single universal Fermi network that predicts ground-state wavefunctions across the family  $\{\hat{H}(\mathbf{\Lambda})\}_{\mathbf{\Lambda} \in \mathcal{P}}$ . The workflow of the entire formalism can be visualized in Fig. 2.

## RESULTS

We evaluate the model on interacting electrons in a two-dimensional harmonic trap across several interaction strengths,  $\lambda$ , and particle numbers,  $N$ . Once the model is optimized through minimizing the energy for a selected set of  $\lambda$ ,  $N$  parameters, it learns to predict the ground state wavefunction for any parameter set over the entire manifold spanned by the training set and even slightly beyond it. The ground state wavefunction is predicted instantaneously by the model, from which static and thermodynamic observables, such as the real space charge density and ground state energy, can be readily computed by Monte Carlo sampling. Here, we emphasize that no further training, transfer learning, or fine tuning is performed; once our foundation model is trained, it can predict many-electron ground states accurately, as we will show below.

TABLE I. Ground state energies for different benchmarked approaches at  $N = 10$ . Energies are produced for same network size as the foundation model, but only trained on one system for the Slater–Jastrow (SJ) backflow, SJ and Hartree–Fock (HF) cases. All SJ backflow, SJ, HF results were trained from scratch. The train column denotes if the Fermi Sets network saw that parameter value during training or not.

$\lambda$	train	Fermi Sets	SJ backflow	SJ	HF
1.0	yes	<b>52.0397</b>	52.0559	52.0796	52.2161
3.0	no	<b>87.5655</b>	87.6543	87.7070	88.7643
5.0	yes	<b>116.9503</b>	117.6311	117.8350	120.4366
7.0	no	<b>142.9216</b>	143.3966	143.8019	149.3424

The main result of this work is demonstrating that a single unified model can accurately predict wavefunctions for Hamiltonians it never saw. Optimizing only on a few interaction strengths  $\lambda \in \{0.0, 1.0, 2.0, 5.0, 8.0, 10.0\}$ , and particle numbers  $N \in \{6, 8, 10\}$ , our model is able to accurately predict the ground state wavefunction throughout the continuous range  $0 \leq \lambda \leq 10.0$ , for every integer  $5 \leq N \leq 11$ . To demonstrate the accuracy, we compare with high-quality variational wavefunctions that are available for small particle numbers. We benchmark our energies against Slater–Jastrow Backflow and Hartree–Fock in Table I. With only a single training run, our predicted energies (seen and unseen) not only outperform these standard quantum Monte Carlo techniques, but also produces a far more accurate ground state wavefunction, as we describe below and in detail in the supplemental material [28]. Moreover, the predicted energies are competitive with diffusion Monte Carlo (DMC) [29] across the full parameter range and surpass both DMC and FermiNet [30] at certain interaction strengths. Importantly, these excellent results are obtained without any problem-specific optimization or supervision: the model is trained purely by unsupervised energy minimization and learns to predict ground states accurately and consistently across interaction strengths and particle numbers.

To demonstrate the quality of the predicted many-body wavefunctions, we plot the predicted one-body density  $n(\mathbf{r}) = N \int d\mathbf{r}_2 \cdots d\mathbf{r}_N \sum_{\mathbf{s}} |\Psi(\mathbf{R}, \mathbf{s})|^2$  in Fig. 3. For  $N = 10$ , the density remains rotationally symmetric for all  $\lambda$ , as expected for a circular dot whose ground state is nondegenerate and has total angular momentum  $L = 0$  (“closed-shell”). Increasing interaction strength  $\lambda$  mainly reshapes the radial profile: repulsion pushes charge density outward and sharpens correlation-driven radial structure, producing the concentric ring features seen from  $\lambda = 1 \rightarrow 7$  [29, 31, 32].

The case  $N = 7$  (bottom row) behaves differently. Here, the noninteracting ground state has a four-fold degeneracy with  $L = \pm 1, \pm 3$  due to one electron filling in the 4-th shell. This “open shell” configuration makes the system susceptible to interaction effects. In-

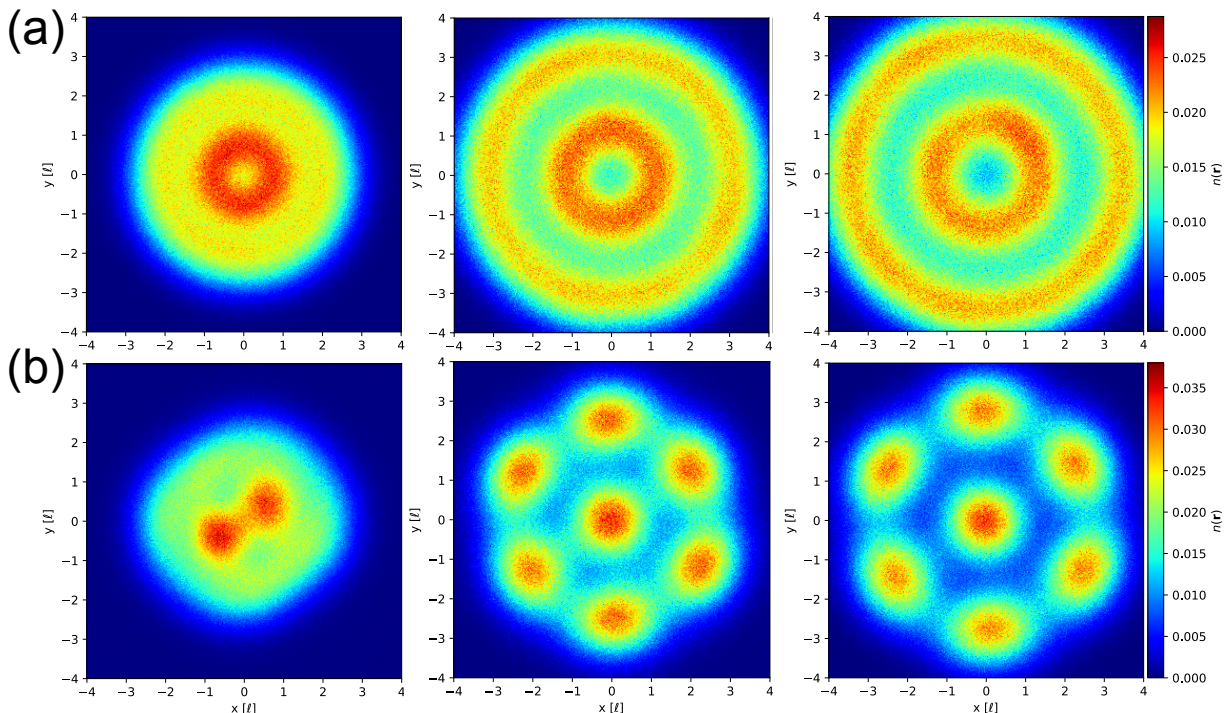


FIG. 3. **Real space particle density from inference for various parameter values.** The first and second row has  $N = 10$  and  $N = 7$ , respectively, with the columns for  $\lambda = 1.0$  (optimized for  $N = 10$ , predicted for  $N = 7$ ),  $5.0$  (optimized for  $N = 10$ , predicted for  $N = 7$ ),  $7.0$  (predicted).

interestingly, the real space charge density of the predicted ground states is not fully rotationally invariant, but shows two-fold symmetry at  $\lambda = 1$  and six-fold symmetry at  $\lambda = 5, 7$ . The rotation symmetry breaking is a consequence of the exact degeneracy between ground states of opposite angular momenta  $+L$  and  $-L$  states, which is guaranteed by time reversal symmetry. The observed charge density shows that the 7-electron ground state changes from  $L = \pm 1$  at weak interaction to  $L = \pm 3$  at strong interaction, in agreement with the finding of a previous full configuration interaction calculation [33]. At strong interaction, the system favors a Wigner-molecule-like arrangement, consistent with the classical  $1 + 6$  configuration expected for  $N = 7$  strongly repelling electrons in a circular confinement [33–37].

These density plots are a stringent wavefunction-level check:  $n(\mathbf{r})$  is a direct functional of  $|\Psi|^2$ , so reproducing the correct symmetry patterns and correlation-driven features across  $\lambda$  and across distinct  $N$  sectors indicates that the foundation model is learning the full landscape of ground-state wavefunctions in parameter space. Minor deviations do exist, which is expected when training targets energy alone, yet these deviations are mostly too small to even be observable. The qualitative and quantitative structure is faithful across particle number and coupling, highlighting the predictive power of the *Large-Electron Model*. With only a few training instances, it recovers the correct symmetry physics and correlation-

induced reorganization of the interacting ground state.

To demonstrate the model’s accuracy over the entire parameter region, we plot the energy calculated from the predicted ground state wavefunction across the  $(\lambda, N)$  grid. Fig. 4 shows that, after optimizing on a small set of parameters, the model produces pinpoint out-of-sample energies for unseen interaction strengths. More strikingly, the same trained parameters generalize across particle number: the model predicts accurate ground-state energies for completely unseen  $N$  values. To our knowledge, this is the first neural quantum state that generalizes across distinct Hilbert-space sectors while yet still producing leading energy accuracy. Previous foundation model studies on molecules and lattice spin models achieved accurate predictions for different Hamiltonian parameters [15, 16, 18, 22], but direct predictions for unseen system sizes were inaccurate and required further fine-tuning [14, 17, 19–21]. We emphasize that our model goes beyond an interpolation effect: all energies are computed from predicted ground states of  $N$  particles, whose Hilbert space changes with  $N$ , yet the same foundation model produces accurate variational results.

Our approach also enables the model to efficiently predict the wavefunction over the entire family of coupling strength for large  $N$ . We find accurate predictions for unseen  $\lambda$ , up to  $N = 50$ , Fig 5, establishing a foundation model for many electrons in the continuum. In this regime, prediction is fast and low-cost: a

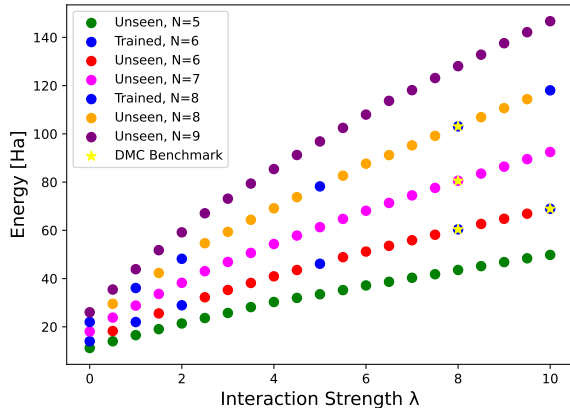


FIG. 4. **Train and Predict results across  $(\lambda, N)$  particle grid.** Model is able to have pinpoint accuracy on out of sample results, able to generate wavefunction and any equal time observable for any parameter, across Hilbert space sectors, at inference time. Energies are competitive with state of the art benchmarks [29], of which a detailed table is provided in the supplementary material [28]. The statistical errors on the energies are far smaller than the radius of the dots, and therefore omitted in the figure.

single trained model can predict across all interaction strengths without re-optimizing from scratch for each parameter point. In the majority of comparisons (for  $6.0 < \lambda < 8.0$ ), the predicted out-of-sample runs outperform freshly trained single-system runs, indicating that parameter-conditioned, multi-task training improves the solution quality rather than diluting it. This is consistent with shared representation learning across the Hamiltonian manifold: training on multiple related systems acts as an inductive bias that stabilizes optimization and improves generalization.

While we demonstrate its performance on quantum dots, our *Large Electron Model* is not tied to this particular system. Indeed, the architecture itself, based on Fermi Sets with parameter conditioning, is completely general and directly applicable to any electron systems, only requiring a specification of  $\hat{H}(\mathbf{\Lambda})$  and a choice of conditioning parameters  $\mathbf{\Lambda}$ . The same model can be trained in the same way on other many-electron settings, such as solids where electrons interact with the nuclei. Taken together, these results establish a direct route to transferrable ground state wavefunctions for real materials: one trained model makes accurate predictions across different materials and configurations.

## CONCLUSION

We introduced a foundation model for real physical systems in the continuum: a single parameter-sharing

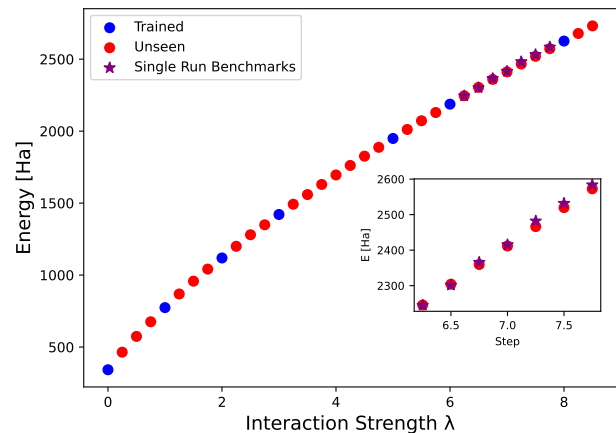


FIG. 5. **Train and Predict Results across for  $N = 50$  over  $\lambda$  parameter manifold.** Model is able to have pinpoint accuracy on out of sample results, able to generate ground state energies that are even lower than single parameter training and evaluation runs (highlighted in the inset). The statistical errors on the energies are far smaller than the radius of the dots, and therefore omitted in the figure.

neural network that maps system and Hamiltonian parameters directly to accurate many-body ground states. By combining a universal fermionic representation with parameter conditioning, the model learns a complete characterization of ground states across systems and Hamiltonian parameters. On interacting electrons in a two-dimensional harmonic trap, the model predicts the accurate many-body wavefunction and produces the state-of-art variational energies and expected charge density.

The central advance is generalization at the wavefunction level. A single trained model predicts accurate many-body ground states for interaction strengths it never saw, and, more importantly, for completely unseen particle numbers. This crosses Hilbert-space sectors where the input dimension and configuration space change, yet the model continues to output accurate Fermi wavefunctions. We further showcase the scaling of our model by generalizing over the entire interaction range, predicting ground state energies for up to  $N = 50$  electrons, and even predicting out-of-sample energies that outperform freshly trained single-system runs, demonstrating that parameter-conditioned training improves model capacity rather than diminishing it.

Because the method is fully unsupervised and requires only the Hamiltonian, it gives a direct route to foundation models for interacting electrons in the continuum, from quantum dots and trapped ions to atoms, molecules, and materials. The result is a powerful and precise formalism that can replace single system workflows with one unified, reusable model, allowing for first principles and large scale studies of real materials.

\* tzaklama@mit.edu

† liangfu@mit.edu

- [1] L. Fu, **Fermi sets: Universal and interpretable neural architectures for fermions** (2026), [arXiv:2601.02508 \[cond-mat.str-el\]](#).
- [2] D. Luo and B. K. Clark, Backflow transformations via neural networks for quantum many-body wave functions, *Phys. Rev. Lett.* **122**, 226401 (2019).
- [3] K. Choo, A. Mezzacapo, and G. Carleo, Fermionic neural-network states for ab-initio electronic structure, *Nat. Commun.* **11**, 1 (2020).
- [4] J. Hermann, Z. Schätzle, and F. Noé, Deep-neural-network solution of the electronic Schrödinger equation, *Nat. Chem.* **12**, 891 (2020).
- [5] D. Pfau, J. S. Spencer, A. G. D. G. Matthews, and W. M. C. Foulkes, Ab initio solution of the many-electron Schrödinger equation with deep neural networks, *Phys. Rev. Res.* **2**, 033429 (2020).
- [6] I. von Glehn, J. S. Spencer, and D. Pfau, A self-attention ansatz for ab-initio quantum chemistry, in *The Eleventh International Conference on Learning Representations* (2023).
- [7] M. Geier, K. Nazaryan, T. Zaklama, and L. Fu, Self-attention neural network for solving correlated electron problems in solids, *Phys. Rev. B* **112**, 045119 (2025).
- [8] Y. Teng, D. D. Dai, and L. Fu, Solving the fractional quantum hall problem with self-attention neural network, *Phys. Rev. B* **111**, 205117 (2025).
- [9] C.-T. Li, T. Ong, M. Geier, H. Lin, and L. Fu, **Attention is all you need to solve chiral superconductivity** (2025), [arXiv:2509.03683 \[cond-mat.supr-con\]](#).
- [10] K. Nazaryan, F. Gaggioli, and L. Fu, Artificial intelligence for quantum matter: Finding a needle in a haystack, [arXiv preprint arXiv:2507.13322](#) (2025).
- [11] A. P. Fadon, D. Pfau, J. S. Spencer, W. T. Lou, T. Neupert, and W. M. C. Foulkes, **Extracting anyon statistics from neural network fractional quantum hall states** (2025), [arXiv:2512.15872 \[cond-mat.str-el\]](#).
- [12] A. Abouelkomsan, M. Geier, and L. Fu, **Topological order in deep state** (2025), [arXiv:2512.01863 \[cond-mat.mes-hall\]](#).
- [13] R. Bommasani *et al.*, **On the opportunities and risks of foundation models** (2021), cRFM Report, Stanford, [arXiv:2108.07258 \[cs.LG\]](#).
- [14] M. Scherbela, R. Reisenhofer, L. Gerard, P. Marquetand, and P. Grohs, Solving the electronic Schrödinger equation for multiple nuclear geometries with weight-sharing deep neural networks, *Nature Computational Science* **2**, 331 (2022).
- [15] N. Gao and S. Günnemann, Ab-initio potential energy surfaces by pairing GNNs with neural wave functions, in *International Conference on Learning Representations* (2022).
- [16] N. Gao and S. Günnemann, Sampling-free inference for ab-initio potential energy surface networks, in *The Eleventh International Conference on Learning Representations* (2023).
- [17] N. Gao and S. Günnemann, Generalizing neural wave functions, in *Proceedings of the 40th International Conference on Machine Learning, ICML'23 (JMLR.org, 2023)*.
- [18] Z. Zhu, M. Mattheakis, W. Pan, and E. Kaxiras, Hubbardnet: Efficient predictions of the bose-hubbard model spectrum with deep neural networks, *Phys. Rev. Res.* **5**, 043084 (2023).
- [19] M. Scherbela, L. Gerard, and P. Grohs, Towards a transferable fermionic neural wavefunction for molecules, *Nature Communications* **15**, 120 (2024).
- [20] L. Gerard, M. Scherbela, H. Sutterud, M. Foulkes, and P. Grohs, **Transferable neural wavefunctions for solids** (2024), [arXiv:2405.07599 \[physics.comp-ph\]](#).
- [21] A. Foster, Z. Schatzle, P. B. Szabo, L. Cheng, J. Kohler, G. Cassalla, N. Gao, J. Li, F. Noe, and J. Hermann, An ab initio foundation model of wavefunctions that accurately describes chemical bond breaking, [arXiv preprint arXiv:2506.19960](#) (2025).
- [22] R. Rende, L. L. Viteritti, F. Becca, A. Scardicchio, A. Laio, and G. Carleo, Foundation neural-networks quantum states as a unified ansatz for multiple hamiltonians, *Nat. Commun.* **16**, 7213 (2025).
- [23] T. Zaklama, D. Guerci, and L. Fu, **Attention-based foundation model for quantum states** (2025), [arXiv:2512.11962 \[cond-mat.str-el\]](#).
- [24] L. Fu, **A minimal and universal representation of fermionic wavefunctions (fermions = bosons + one)** (2025), [arXiv:2510.11431 \[cond-mat.str-el\]](#).
- [25] D. Pfau, J. S. Spencer, A. G. D. G. Matthews, and W. M. C. Foulkes, Ab initio solution of the many-electron Schrödinger equation with deep neural networks, *Phys. Rev. Research* **2**, 033429 (2020).
- [26] A. Avdoshkin, M. Geier, and L. Fu, **An integrated neural wavefunction solver for spinful fermi systems** (2025), [arXiv:2510.18621 \[quant-ph\]](#).
- [27] I. von Glehn, J. S. Spencer, and D. Pfau, A self-attention ansatz for ab-initio quantum chemistry, [arXiv](#) (2022), [arXiv:2211.13672 \[physics.chem-ph\]](#).
- [28] See supplementary Material at url .... for a details on....
- [29] A. Ghosal, A. D. Güçlü, C. J. Umrigar, D. Ullmo, and H. U. Baranger, Incipient wigner localization in circular quantum dots, *Phys. Rev. B* **76**, 085341 (2007).
- [30] A. Perez Fadon, G. Cassella, H. Sutterud, and W. M. C. Foulkes, Interaction-induced symmetry breaking in circular quantum dots, *The Journal of Chemical Physics* **162**, 154305 (2025), <https://pubs.aip.org/aip/jcp/article-pdf/doi/10.1063/5.0256827/20490273/15430515.0256827.pdf>.
- [31] B. Reusch, W. Häusler, and H. Grabert, Wigner molecules in quantum dots, *Phys. Rev. B* **63**, 113313 (2001).
- [32] F. Pederiva, C. J. Umrigar, and E. Lipparini, Diffusion monte carlo study of circular quantum dots, *Phys. Rev. B* **62**, 8120 (2000).
- [33] M. Rontani, C. Cavazzoni, D. Bellucci, and G. Goldoni, Full configuration interaction approach to the few-electron problem in artificial atoms, *The Journal of Chemical Physics* **124**, 124102 (2006), <https://pubs.aip.org/aip/jcp/article-pdf/doi/10.1063/1.2179418/15382134/124102online.pdf>.
- [34] C. Yannouleas and U. Landman, Spontaneous symmetry breaking in single and molecular quantum dots, *Phys. Rev. Lett.* **82**, 5325 (1999).
- [35] S. M. Reimann and M. Manninen, Electronic structure of quantum dots, *Rev. Mod. Phys.* **74**, 1283 (2002).
- [36] J. Mitroy, S. Bubin, W. Horiuchi, Y. Suzuki, L. Adamowicz, W. Cencek, K. Szalewicz, J. Komasa, D. Blume, and K. Varga, Theory and application of explicitly correlated

- gaussians, *Rev. Mod. Phys.* **85**, 693 (2013).
- [37] J. A. Sheikh, J. Dobaczewski, P. Ring, L. M. Robledo, and C. Yannouleas, Symmetry restoration in mean-field approaches, *Journal of Physics G: Nuclear and Particle Physics* **48**, 123001 (2021).

# Supplementary Material for *Large Electron Model: A Universal Ground State Predictor*

Timothy Zaklama<sup>1</sup>, Max Geier<sup>1</sup>, and Liang Fu<sup>1</sup>

<sup>1</sup>*Department of Physics, Massachusetts Institute of Technology, Cambridge, MA-02139, USA*

## CONTENTS

I. Table of benchmarked energies	2
II. Slater-Jastrow and Hartree Fock Comparison	2
III. Optimization stability across system size	4
IV. Extended Data	5

## I. Table of benchmarked energies

TABLE II. Benchmarked energies for trained inference compared with DMC and FermiNet references.

$\lambda$	$N$	Fermi Sets	DMC [29]	FermiNet [30]
8.0	6	<b>60.3748</b>	60.3924	60.402
10.0	6	68.9584	<b>68.9458</b>	68.967
8.0	7	80.5328	<b>80.5146</b>	80.528(3)
8.0	8	103.065	<b>103.0464</b>	103.0467

The estimated energies from our *Large Electron Model* are produced all at once from a single run. In principle, the model can be further trained to optimize a single ground state energy after the run on many different parameter values, which would produce even lower energies.

## II. Slater-Jastrow and Hartree Fock Comparison

Figure S1 compares one-body densities at  $\lambda = 1.0, 3.0, 7.0$  obtained from two standard baselines: a Slater–Jastrow trial state (top row) and Hartree–Fock (bottom row). For a circular quantum dot, the Hamiltonian is rotationally invariant, and thus it commutes with the total angular-momentum operator

$$\hat{L}_z = \sum_{i=1}^N \hat{\ell}_{z,i} = -i \sum_{i=1}^N \frac{\partial}{\partial \theta_i}, \quad [\hat{H}, \hat{L}_z] = 0. \quad (\text{S1})$$

Exact eigenstates may therefore be chosen with definite total angular momentum  $L$ , and the corresponding one-body density

$$n(\mathbf{r}) = \left\langle \Psi \left| \sum_{i=1}^N \delta(\mathbf{r} - \mathbf{r}_i) \right| \Psi \right\rangle \quad (\text{S2})$$

is rotationally symmetric for a single  $L$  sector. Angular modulation in  $n(\mathbf{r})$  arises when the approximate state mixes angular-momentum sectors (or forms a real linear combination of near-degenerate  $\pm L$  sectors) according to

$$n(\theta) = \frac{1}{2\pi} \left( 1 + 2|ab^*| \cos(2l\theta + \arg(ab^*)) \right), \quad (\text{S3})$$

for amplitudes  $a, b$  of nearly degenerate  $\pm L$  sectors, which is precisely the failure mode highlighted by the Hartree–Fock densities at stronger coupling.

Hartree–Fock approximates the many-body state by a single Slater determinant,

$$\Psi_{\text{HF}}(\mathbf{R}, \mathbf{s}) = \det[\chi_j(\mathbf{r}_i, s_i)], \quad n_{\text{HF}}(\mathbf{r}) = \sum_{j=1}^N |\chi_j(\mathbf{r})|^2, \quad (\text{S4})$$

and treats interactions at the mean-field exchange level. At weak coupling ( $\lambda = 1.0$ ), the density remains close to circular because the single-determinant picture is still reasonable. As  $\lambda$  increases, correlations dominate and the mean-field solution lowers its energy by spontaneously localizing the orbitals, producing an azimuthally modulated, symmetry-broken charge density. At  $\lambda = 7.0$  the Hartree–Fock density becomes strongly non-uniform and irregular, reflecting that the self-consistent orbitals are not eigenstates of angular momentum but rather superpositions of many  $m$  components; the determinant therefore mixes many total- $L$  sectors, and the one-body density no longer represents a controlled approximation to the rotationally invariant ground-state density. In this regime Hartree–Fock should be viewed as a broken-symmetry mean-field picture of localization rather than a faithful correlated eigenstate.

The Slater–Jastrow baseline partially repairs this by introducing explicit correlations on top of a determinant,

$$\Psi_{\text{SJ}}(\mathbf{R}, \mathbf{s}) = \exp(J(\mathbf{R})) \det[\phi_j(\tilde{\mathbf{r}}_i, s_i)], \quad J(\mathbf{R}) = \sum_{i < j} u(r_{ij}) + \sum_i \nu(r_i) + \dots, \quad (\text{S5})$$

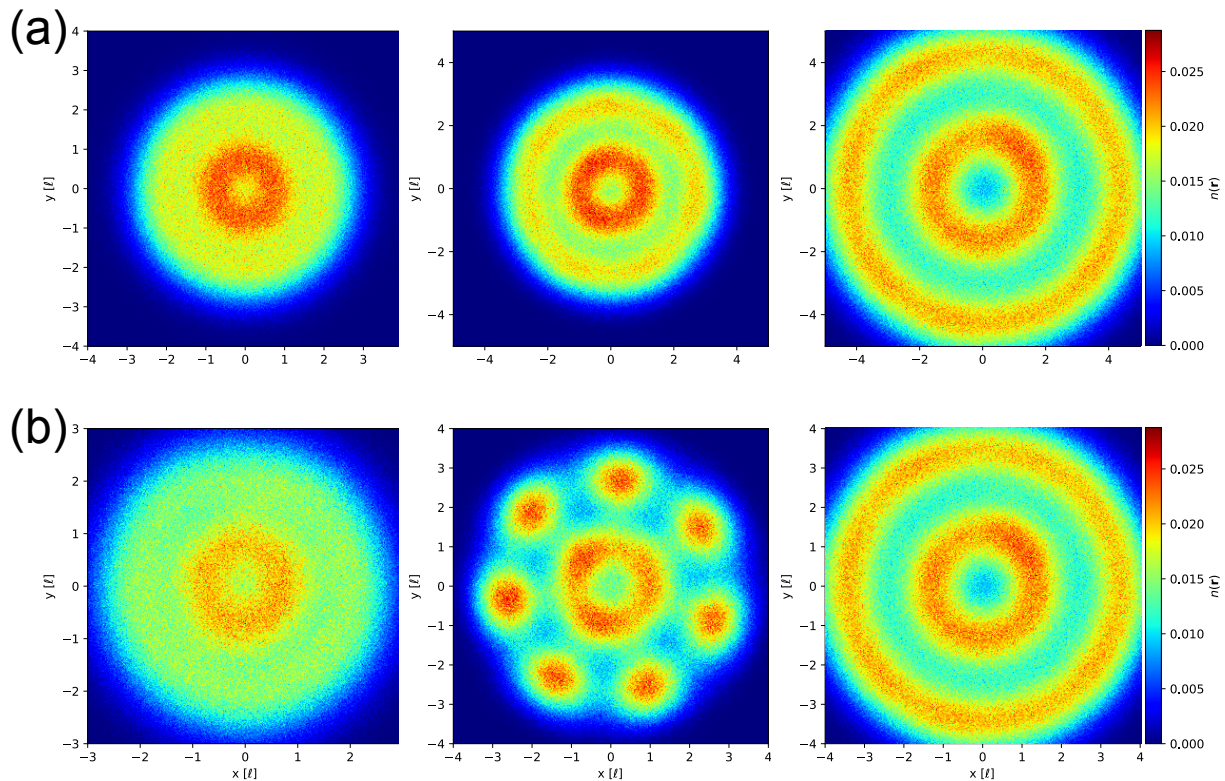


FIG. S1. Real space particle density for Slater-Jastrow (a) and Hartree-Fock (b) calculations at  $N = 10, \lambda = 1.0, 3.0, 7.0$ .

where we have the option to integrate a backflow component to further improve the nodal structure, and recover even more correlation energy. The backflow coordinates  $\tilde{\mathbf{r}}_i$  are smooth, permutation-equivariant displacements of the bare electron positions that depend on the full configuration,

$$\tilde{\mathbf{r}}_i = \mathbf{r}_i + \sum_{j \neq i} \eta(r_{ij}) (\mathbf{r}_i - \mathbf{r}_j) + \dots, \quad (\text{S6})$$

(with  $\eta$  a learned or parameterized scalar function). The Jastrow factor captures the short-range correlation hole and a substantial fraction of dynamic correlation, while backflow improves the nodal structure by allowing the determinant to depend on correlation-distorted coordinates. This is reflected in Fig. S1: compared to Hartree-Fock, the Slater-Jastrow (no backflow) densities remain closer to the expected circular profile at weak and intermediate coupling, and when angular features appear at strong coupling they do so in a more regular, physically interpretable pattern. However, even with backflow the ansatz remains limited by its restricted determinant backbone and cannot represent the full multiconfigurational mixing that becomes essential in the strongly correlated regime (also making it unstable and difficult to optimize at higher couplings). As a result, Slater-Jastrow can still exhibit residual angular-momentum mixing and does not match the wavefunction-level fidelity achieved by the foundation model.

In contrast, our Fermi Sets foundation model retains a compact antisymmetric core while learning correlations through a symmetric, configuration- and parameter-dependent mixing of antisymmetric components. This allows the model to represent correlation-driven reorganization without relying on uncontrolled symmetry breaking, and it produces densities that track the ground-state structure across  $\lambda$  and across particle-number sectors. The comparison in Fig. S1 therefore serves as a wavefunction-level diagnostic: Hartree-Fock breaks down first and most severely, Slater-Jastrow (backflow) captures a large portion of correlations but remains limited by its fixed antisymmetric (determinant) backbone, and the Fermi Sets foundation model provides the most faithful densities consistent with its superior energy accuracy. Comparison of energies is shown in Table I.

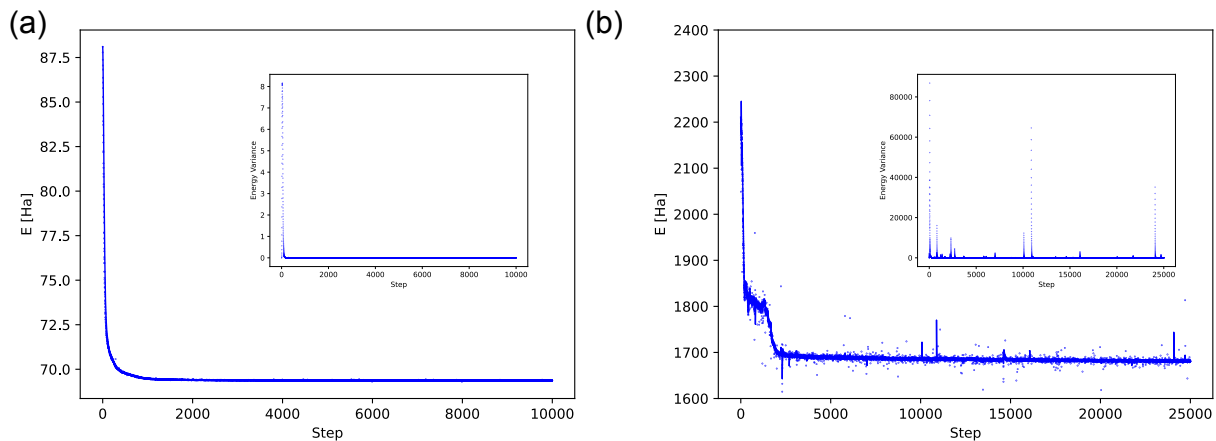


FIG. S2. **Total loss and variance for small particle number run in main text for (a)  $N = 6, 8, 10, \lambda = 0.0, 1.0, 2.0, 5.0, 8.0, 10.0$  and (b)  $N = 50, \lambda = 0.0, 1.0, 2.0, 3.0, 5.0, 6.0, 8.0, 10.0$ .**

### III. Optimization stability across system size

Figure S2 compares optimization behavior for a co-trained small- $N$  model (18 parameter groups spanning  $N \in \{6, 8, 10\}$  and  $\lambda \in \{0.0, 1.0, 2.0, 5.0, 8.0, 10.0\}$ ) and a large- $N$  model ( $N=50, \lambda \in \{0.0, 1.0, 2.0, 3.0, 5.0, 6.0, 8.0, 10.0\}$ ). The plotted loss is the mean variational energy, averaged over all parameter groups (explicitly shown in eq. 5, and the insets show the corresponding energy variance. Despite training on more systems, the small- $N$  run is markedly stable: the loss drops rapidly and plateaus early, and the variance collapses quickly. The large- $N$  run is noisier and converges more slowly, with occasional spikes in both the energy and variance. This behavior is expected in the large-electron regime: model memory and compute scale roughly as  $N^2$  through pairwise features and determinant construction, and with a single 96 GB GPU, we must constrain batch size and model width. Even with these constraints, the optimization remains well behaved at long times and the final energies achieve high accuracy, with typical standard errors below  $10^{-3}$  on average.

Figure S3 resolves the same training into per-parameter curves. For the small- $N$  co-training (top panel), each  $(N, \lambda)$  group converges smoothly with only mild transient noise. For the large- $N$  co-training (bottom panel), the relative ordering of noise across  $\lambda$  differs from single-task training: lower  $\lambda$  runs exhibit visibly larger fluctuations than higher  $\lambda$  runs. This does not reflect increased physical difficulty at weak coupling; it is an optimization effect induced by simultaneous training across tasks with widely separated energy scales. When the objective is averaged across parameter groups,

$$\mathcal{L}(\theta) = \frac{1}{G} \sum_{g=1}^G E_{\theta}(\mathbf{p}_g), \quad E_{\theta}(\mathbf{p}_g) = \mathbb{E}_{(\mathbf{R}, \mathbf{s}) \sim |\Psi_{\theta}(\cdot; \mathbf{p}_g)|^2} [E_L(\mathbf{R}, \mathbf{s}; \mathbf{p}_g)], \quad (\text{S7})$$

groups with larger absolute energies (typically larger  $\lambda$  and/or larger  $N$ ) contribute gradients with larger magnitude, setting an effective step scale for the shared parameters. For smaller- $\lambda$  groups, this can act like an overly aggressive step size, producing higher apparent noise even when those tasks are individually easy.

This effect can be reduced by balancing the multi-task optimization. One option is to reweight the loss by a  $\lambda$ -dependent factor or by a running estimate of task scale, e.g. normalizing each group by an energy or variance scale so that gradients are comparable across  $\mathbf{p}_g$ . Another option is to add a weak regularizer that suppresses excess variance in low- $\lambda$  groups during co-training, or to increase model capacity when resources allow, which reduces competition between tasks and lowers gradient interference. In practice, the observed noise does not prevent accurate convergence: the large- $N$  model still reaches stable final energies and produces highly faithful predicted wavefunctions across the full coupling range, demonstrating that parameter-conditioned co-training remains effective even in the most memory-constrained regime.

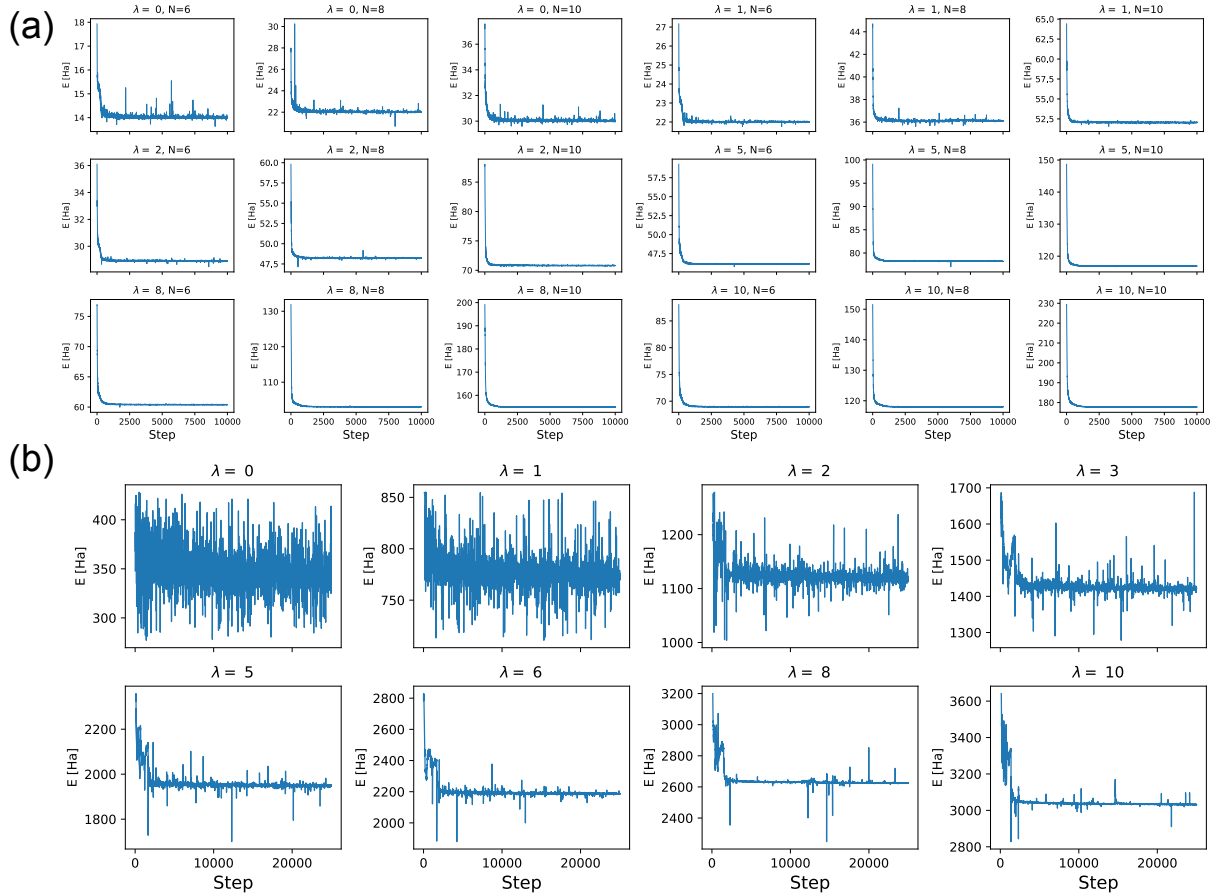


FIG. S3. Group loss for each parameter group in the runs in the main text, also corresponding to the runs in Fig S2

#### IV. EXTENDED DATA

Fig. S4 provides a direct visualization of the full many-body wavefunction,  $\Psi_{\theta}(\mathbf{r}_1, \dots, \mathbf{r}_N)$ , of the model, which we include to again emphasize the model's learning of the full-many body wavefunction rather than some cheap derivative. For each system we construct a *conditional wavefunction slice* by fixing  $N-1$  electron coordinates at a representative high-probability configuration (white markers) and scanning the remaining coordinate  $\mathbf{r}$  across the 2D plane. The left column shows the conditional probability density  $|\psi_{\text{cond}}(\mathbf{r})|^2 \propto |\Psi_{\theta}(\mathbf{r}, \mathbf{r}_2^*, \dots, \mathbf{r}_N^*)|^2$ , while the middle column shows the corresponding phase  $\phi(\mathbf{r}) = \arg \psi_{\text{cond}}(\mathbf{r})$ . The sharp boundaries between phase domains coincide with suppressed amplitude and identify nodal contours of the many-body state, information that is inaccessible from one-body densities alone and is not fixed by matching energies. In particular, the presence and topology of these nodal domains demonstrates that the model captures the sign/phase structure (and thus fermionic antisymmetry) of the ground state.

The right column reports the pair correlation function  $g(\mathbf{r})$  (conditional density relative to a reference electron, placed at center of plot), connecting the wavefunction-level visualization to a standard reduced observable. For the full-shell case  $N = 10$  at  $\lambda = 8$  (top row),  $g(\mathbf{r})$  exhibits a pronounced exchange-correlation hole at short distance and an approximately isotropic correlation ring, consistent with the rotationally symmetric density profile expected for a filled shell. For the open-shell case  $N = 7$  at  $\lambda = 8$  (bottom row),  $g(\mathbf{r})$  shows the same correlation hole but with stronger angular modulation and enhanced localization, reflecting the increased role of correlations in an incompletely filled shell. Importantly, these anisotropic features appear in conditional objects ( $\psi_{\text{cond}}$  and  $g$ ) while remaining consistent with the rotationally symmetric one-body densities shown in the main text: averaging over particle labels and configurations restores rotational symmetry even when individual conditional slices reveal structured nodal and correlation patterns.

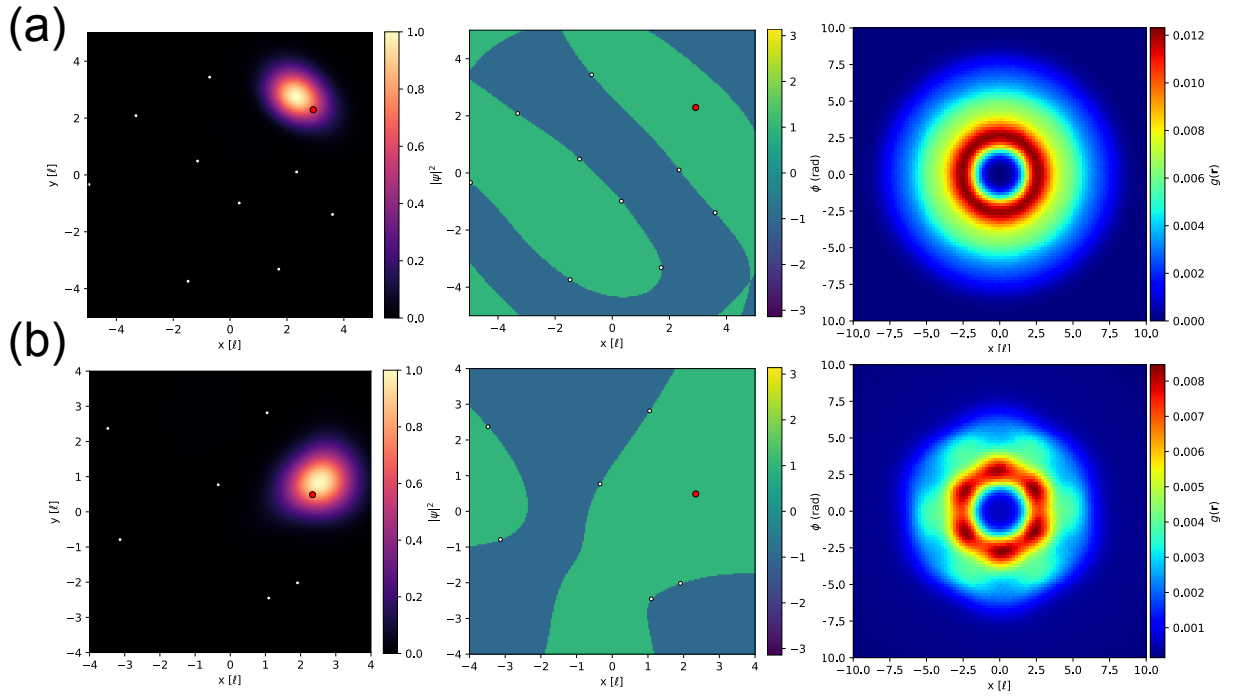


FIG. S4. Conditional probability (left), phase (middle), and pair correlation plot (right) for (a)  $N = 10$  and (b)  $N = 7$  for  $\lambda = 8.0$ .